Korean J. Chem. Eng., 35(2), 355-363 (2018)
DOI: 10.1007/s11814-017-0295-7

pISSN: 0256-1115
eISSN: 1975-7220

Maximum production of methanol in a pilot-scale process

Minji Son*, Myung-June Park*,,†, Geunjae Kwak***, Hae-Gu Park***, and Ki-Won Jun*****

*Department of Energy Systems Research, Ajou University, Suwon 16499, Korea
**Department of Chemical Engineering, Ajou University, Suwon 16499, Korea
***C1 Gas Conversion Research Group, Carbon Resources Institute,
Korea Research Institute of Chemical Technology (KRICT), Daejeon 34114, Korea
(*Received 11 September 2017 • accepted 15 October 2017*)

Abstract−Mathematical models for both bench- and pilot-scale methanol synthesis reactors were developed by estimating the overall heat transfer coefficients due to different heat transfer characteristics, while the effectiveness factor was fixed because the same catalysts were used in both reactors. The overall heat transfer coefficient of a pilot-scale reactor was approximately twice that of a bench-scale reactor, while the estimate from the correlation reported for the heat transfer coefficient was 1.8-times higher, indicating that the values determined in the present study are effective. The model showed that the maximum methanol production rate of approximately 16 tons per day was achievable with peak temperature maintained below 250 °C in the open-loop case. Meanwhile, when the recycle was used to prevent the loss of unreacted gas, peak temperature and production rate decreased due to low CO and CO_2 fraction in the recycled stream at the same space velocity as the open-loop operation. Further analysis showed that, since the reaction was in the kinetic regime, the production rate could be maximized up to 18.7 tons per day by increasing the feed flowrate and inlet temperature despite thermodynamically exothermic reaction.

Keywords: Methanol, Reactor Modeling, Effectiveness Factor, Overall Heat Transfer Coefficient, Maximum Production

INTRODUCTION

Interest in methanol production and demand for methanol are expected to increase further in the next several decades due to the rapidly growing demand for alternative clean energy. Methanol is used extensively as a raw material for the production of chemicals such as formaldehyde, methyl tert-butyl ether (MTBE), and acetic acid. It can also be used to produce electricity by direct oxidization with air to water and carbon dioxide in a direct methanol fuel cell (DMFC) [1,2]. Methanol is also an excellent fuel in its own right and can be converted conveniently into ethylene or propylene through the methanol-to-olefins (MTO) process [3-5].

Several catalysts, based on Cu, Zn, Cr, and Pd, have been reported to maximize both the yield and selectivity of methanol and to prevent the formation of hydrocarbons. Among these, Cu/ZnO catalysts are well-known for their high activity and selectivity, which can be increased further by using a support such as Al_2O_3 [6-8].

To remove the heat released by the highly exothermic methanol synthesis reaction efficiently, many studies have focused on kinetics and reactor modeling when designing commercial processes for mass production [4]. Because the roles of CO and CO_2 have not been defined clearly, several kinetic models have been suggested based on different reaction pathways and conditions. Natta assumed that CO hydrogenation is the only mechanism for the production of methanol and suggested the corresponding reversible reaction rate [9,10]. Takagawa et al. [11] considered both CO and CO_2 hydrogenations on the basis of experimental results with varying CO and CO_2 ratios over a Cu/Zn catalyst and determined the kinetic parameters for the reaction rates of the CO and CO_2 hydrogenations and reverse water gas shift (WGS) reaction. Peter et al. developed a power-law model, a Langmuir-Hinshelwood-Hougen-Watson (LHHW) model, and a microkinetic model and conducted a sensitivity analysis to evaluate the effects of kinetic parameters on methanol formation rate [12]. In our previous works [6,13], four reactions were considered over a $Cu/ZnO/Al_2O_3$ catalyst, CO and CO_2 hydrogenations, WGS reaction, and dimethyl ether (DME) formation, where the surface reaction of a methoxy species, the hydrogenation of a formate intermediate HCO_2, and the formation of a formate intermediate were shown to be the rate determining steps for CO and CO_2 hydrogenations and WGS reaction, respectively. Recently, the Monte Carlo method has been applied in the methanol synthesis reaction over Cu(111) catalysts to evaluate the dependence of conversion and selectivity on the operating conditions [14].

Løvik et al. [15] did dynamic modeling and optimization for a typical methanol synthesis reactor, when catalyst deactivation existed, and suggested a strategy for the optimal temperature trajectory for maximum methanol productivity. Kordabadi and Jahanmiri [16] applied the genetic algorithm to maximize methanol production yield, and suggested a reactor with optimal two-stage cooling shells that resulted in an increase of yield of 2.9% during the operating period. They also applied the same strategy to a methanol synthesis reactor when catalyst deactivation existed and reduced the degree of deactivation by applying a multi-objective genetic algorithm [17]. Lim et al. [18] showed that the optimal CO_2 fraction for maximum

†To whom correspondence should be addressed.
E-mail: mjpark@ajou.ac.kr

methanol production is a function of temperature and thus calculated the optimal CO_2 fractions for each catalytic bed for a three-stage methanol synthesis reactor over a $Cu/ZnO/Al_2O_3/ZrO_2$ catalyst. Zhang et al. modeled a gas-to-methanol process using a process simulator (Aspen Plus), and analyzed the effects of CO_2 feeding on the techno-economics of the entire process [19].

We considered mathematical modeling to evaluate the effects of operating conditions and suggest an optimal condition for maximum methanol production in a pilot-scale (10 ton per day production of methanol) reactor. Since the conditions in the pilot-scale operation are limited while data under various operating conditions are required to estimate parameters in the model, an effectiveness factor and overall heat transfer coefficients were determined using experimental data from a bench-scale reactor with commercial pellet-type catalysts. The model with the same effectiveness factor was used further in the modeling of a pilot-scale reactor with the same type of catalysts, while the overall heat transfer coefficient was re-estimated due to different operating conditions (high linear velocity of feed gas compared to a bench-scale operation).

EXPERIMENTAL

1. Catalyst Preparation

A commercial $CuO/ZnO/Al_2O_3$ catalyst from Dalian Reak Science & Technology was used in all methanol synthesis experiments. According to the vendor-supplied details for the catalyst, the catalyst has a molar ratio of Cu/Zn/Al=60/30/10, a cylindrical shape (5 mm diameter and 5 mm height), and a bulk density of 1.1-1.3 kg/L. The catalyst was loaded into the reactors as received without any pre-treatment or crushing. Prior to the reaction, the loaded catalyst was reduced at 250 °C for 4 h in a flow of 5% H_2 balanced with nitrogen. After reduction, the synthesis gas was fed into the reactor.

2. Bench-scale Reactor

A schematic of the bench-scale reactor is provided in Fig. 1. A tube (diameter and length of 5.15 cm and 212 cm, respectively) was filled with inert material (upper part, 142 cm long) and catalyst material (60 cm long, 100 g catalyst and 2,200 g inert), and five temperature detectors were installed at the center of the catalytic bed (detailed locations are shown in Fig. 1). Experiments were conducted at 50 and 60 bar, while temperature (inlet and wall) and space velocity were specified to be 225 °C and 8,000 mL/(g_{cat}·h), respectively. The composition of the feed gas was 24%, 6%, 64%, and 6% CO, CO_2, H_2, and Ar, respectively.

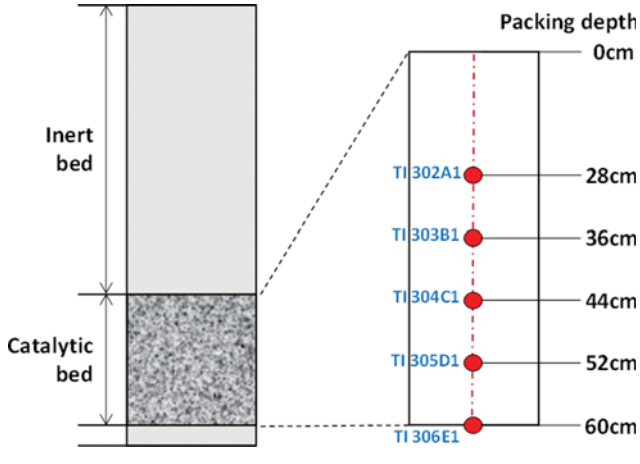

Fig. 1. Scheme of the bench-scale reactor and locations of temperature detectors in the catalytic bed.

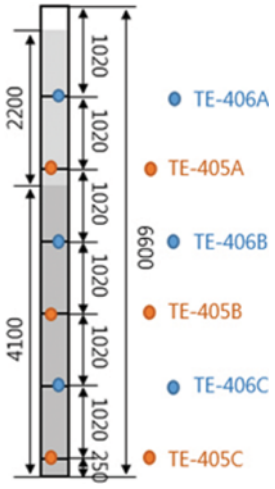

Fig. 2. Scheme of the pilot-scale methanol synthesis reactor.

3. Pilot-scale Reactor

A schematic of the pilot-scale methanol synthesis system is provided in Fig. 2. The upper part of a tube (inner diameter and length of 4.1 cm and 6.37 m, respectively) was filled with catalysts (1.58 kg per tube) and inerts (2.77 kg per tube) in order to prevent abrupt temperature increase, and the lower part was filled only with catalysts (6.1 kg per tube). The corresponding packing depths were 2.2 and 4.1 m for the upper and lower parts, respectively. The total number of tubes was 82. The pressure and temperature were specified to be 78.2 bar and 184 °C, respectively, and the space velocity was 6,365 mL/(g_{cat}·h). The feed composition was 8.8%, 9.8%, 59.2%, and 22.2% CO, CO_2, H_2, and CH_4, respectively. The composition of the bench-scale reactor was close to that in the lab-scale reactor in our previous study [13], while pilot-scale reactor was developed to use by-product gas in an industry. Therefore, the composition was changed to the value close to that of by-product gas.

RESULTS AND DISCUSSION

1. Kinetic Model for Powder Catalyst in a Lab-scale Reactor

The overall reaction mechanism for methanol synthesis is as follows:

$$\text{CO hydrogenation: } CO + 2H_2 \rightleftharpoons CH_3OH \quad (1)$$

$$\text{CO_2 hydrogenation: } CO_2 + 3H_2 \rightleftharpoons CH_3OH + H_2O \quad (2)$$

$$\text{Reverse water-gas shift: } CO_2 + H_2 \rightleftharpoons CO + H_2O \quad (3)$$

$$\text{DME production: } 2CH_3OH \rightleftharpoons CH_3OCH_3 + H_2O \quad (4)$$

The reaction rates for each reaction are available in our previous work [13]; Table 1 summarizes the reported values of the kinetic parameters, which were used without further modification in the present study:

Table 1. Kinetic parameters for a lab-scale methanol synthesis reactor available in the literature

Parameter	Unit	Value	Remark
k_A	$mol/(kg_{cat}\cdot s\cdot bar^{1.5})$	$1.88\times10^{8}\exp\left(\frac{-113{,}711}{RT}\right)$	[13]
k_B	$mol/(kg_{cat}\cdot s\cdot bar)$	$1.16\times10^{10}\exp\left(\frac{-126{,}573}{RT}\right)$	
k_C	$mol/(kg_{cat}\cdot s\cdot bar^{1.5})$	$7.08\times10^{4}\exp\left(\frac{-68{,}252}{RT}\right)$	
k_{DME}	$mol/(kg_{cat}\cdot s)$	$8.54\times10^{9}\exp\left(\frac{-123{,}779}{RT}\right)$	
K_{H_2O}	bar^{-1}	$3.80\times10^{-10}\exp\left(\frac{80{,}876}{RT}\right)$	
K_{CO}	bar^{-1}	$8.00\times10^{-7}\exp\left(\frac{-58{,}015}{RT}\right)$	[23]
K_{H_2}	bar^{-1}	$27.08\exp\left(\frac{6{,}291}{RT}\right)$	
K_{CO_2}	bar^{-1}	$1.02\times10^{-7}\exp\left(\frac{-67{,}439}{RT}\right)$	
$K_{P,A}$	bar^{-2}	$2.39\times10^{-13}\exp\left(\frac{-98{,}379}{RT}\right)$	
$K_{P,B}$	-	$1.02\times10^{2}\exp\left(\frac{39{,}685}{RT}\right)$	
$K_{P,C}$	bar^{-2}	$2.56\times10^{-11}\exp\left(\frac{-58{,}695}{RT}\right)$	
$K_{P,DME}$	bar^{-2}	$0.106\exp\left(\frac{21{,}858}{RT}\right)$	[24]
K_{CH_3OH}	$m^3/kmol$	$7.90\times10^{-4}\exp\left(\frac{70{,}500}{RT}\right)$	
$K_{H_2O,DME}$	$m^3/kmol$	$8.40\times10^{-2}\exp\left(\frac{41{,}100}{RT}\right)$	

$$r_{CO}=\frac{k_A K_{CO}[f_{CO}f_{H_2}^{1.5}-f_{CH_3OH}/(K_{P,A}f_{H_2}^{0.5})]}{(1+K_{CO}f_{CO})(1+K_{H_2}^{0.5}f_{H_2}^{0.5}+K_{H_2O}f_{H_2O})} \quad (5)$$

$$r_{CO_2}=\frac{k_C K_{CO_2}[f_{CO_2}f_{H_2}^{1.5}-f_{H_2O}f_{CH_3OH}/(K_{P,C}f_{H_2}^{0.5})]}{(1+K_{CO_2}f_{CO_2})(1+K_{H_2}^{0.5}f_{H_2}^{0.5}+K_{H_2O}f_{H_2O})} \quad (6)$$

$$r_{RWGS}=-\frac{k_B K_{CO_2}[f_{CO_2}f_{H_2}-f_{CO}f_{H_2O}/K_{P,B}]}{(1+K_{CO_2}f_{CO_2})(1+K_{H_2}^{0.5}f_{H_2}^{0.5}+K_{H_2O}f_{H_2O})} \quad (7)$$

$$r_{DME}=\frac{k_{DME}K_{CH_3OH}^{2}[C_{CH_3OH}^{2}-(C_{H_2O}C_{DME})/K_{P,DME}]}{(1+2\sqrt{K_{CH_3OH}C_{CH_3OH}}+K_{H_2O,DME}C_{H_2O})^{4}} \quad (8)$$

Here, f denotes the fugacity, which was calculated using the generalized correlations for the fugacity coefficient in the literature [20], and K_p represents the reaction equilibrium constant (values in Table 1). In the case of the DME production rate, C_i was the concentration of component i in mol/m^3.

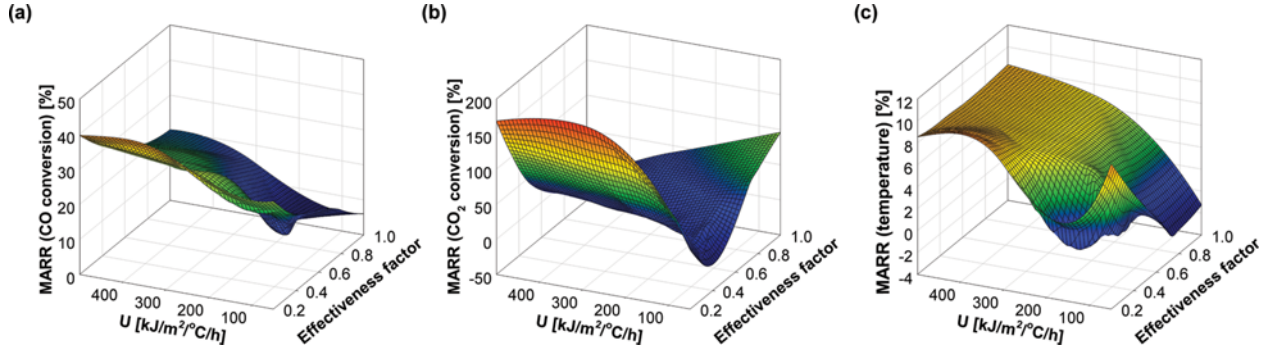

Fig. 3. Effects of overall heat transfer coefficient (U) and effectiveness factor (η) on the mean of absolute relative residual (MARR) of (a) CO conversion, (b) CO_2 conversion, and (c) temperature profiles (averaged value of five measurement points) in a bench-scale reactor.

Table 2. MARR values as a function of effectiveness factor and overall heat transfer coefficient in a bench-scale reactor

No.	Effectiveness factor (η)	Overall heat transfer coefficient (U)	MARR [%]			Remark
			Temperature	CO conversion	CO_2 conversion	
1	0.2	300	7.4	38.7	184.4	50 bar
2	0.4		7.2	28.6	60	
3	0.6		7.1	22.8	7.8	
4	0.8		7.1	18.4	21.2	
5	1		7	14.8	40.1	
6	0.3	500	8.3	35.2	119.1	
7		300	7.3	32.7	106	
8		100	1.6	23.5	50.7	
9		50	7	25.6	2.1	
10	0.4	100	1.4	19.5	12.8	
11		90	0.6	19	6.5	
12		80	1.4	18.9	0.8	
13	0.5	500	8.2	28.1	39.7	
14		400	7.8	27.1	35.8	
15		300	7.2	25.4	29.5	
16		200	5.9	22.3	17.6	
17		130	3.5	18.3	0.5	
18		126	3.3	18	1	
19		122	3	17.7	2.5	
20		118	2.8	17.5	4.1	
21		114	2.5	17.2	5.7	
22		110	2.3	17	7.5	
23		105	1.8	16.7	9.8	
24		100	1.4	16.5	12.4	
25	0.6	500	8.1	25.6	17.1	
26		300	7.1	22.8	7.8	
27		200	5.8	19.6	3	
28		180	5.3	18.6	6.4	
29		150	4.4	16.8	13	
30		100	1.2	14.1	30.8	
31	0.7	500	8.1	23.4	0.1	
32		300	7.1	20.5	8.5	
33		200	5.8	17.1	18.6	
34		100	1.2	12.1	45.3	
35	0.5	130	3.1	7.7	16.8	60 bar
36		126	2.5	7.5	18.2	
37		122	2.2	7.4	19.7	
38		118	1.9	7.3	21.3	
39		114	1.5	7.2	23	
40		110	1.2	7.2	24.8	
41		105	0.9	7.3	27.1	
42		100	0.8	7.4	29.6	
43	0.6	200	5.5	8.7	17.6	
44		180	4.9	7.6	21.2	
45		150	3.8	6	28.1	
46	0.7	200	5.5	6.2	31.5	

The above rate equations were applied to a process simulator (UniSim Design Suite, Honeywell Inc.) to simulate a plug flow reactor (PFR). To obtain the axial profiles in the PFR, the reactor was divided into several subvolumes where the reaction rates were considered to be spatially uniform. A mole balance was done at steady state in each subvolume j as follows:

$$F_{j0} - F_j + r_j V = 0 \quad (9)$$

2. Bench-scale Reactor Modeling

To consider the mass transfer resistance resulting from the increase of particle size (from powder to pellet type), an effectiveness factor (η) was considered. In addition, because the different particle size led to a change of porosity of the catalytic bed, the overall heat transfer coefficient (U) was also determined to explain the different characteristics of heat transfer in a bench-scale reactor.

Fig. 3 shows the effects of η and U on the conversion and temperature profiles in the catalytic bed (detailed values are provided in Table 2). The mean absolute relative residual (MARR) of CO_2 conversion was relatively large compared to those of CO conversion and temperature, probably due to the small values of experimental data in the denominators. For both pressure conditions, an effectiveness factor of 0.5 and an overall heat transfer coefficient of 122 kJ/(m^2·°C·h) were determined to be the most adequate values from the perspective of balanced estimation; comparisons between experimental data and simulated results are provided in Fig. 4, together with the values of relative errors. Note that although the reaction rate for DME production was considered in our previous work, negligible amount of DME was measured in experimental data of the present study. Therefore, DME production was ignored in the determination of η and U.

There are two kinds of effectiveness factors: internal and overall. To evaluate the contribution of internal and external mass transfer resistance, the dimensionless Mears parameters were calculated under all the experimental conditions and the values were less than 3.75×10^{-8} (much lower than the threshold value of 0.15), confirming negligible external mass diffusion [21]. Meanwhile, dimensionless Weisz-Prater parameters (C_{WP}) were calculated to be 0.02 (higher than the threshold value of 0.01), indicating the existence of internal diffusion limitation. Therefore, the effectiveness factor in the present study represents internal one.

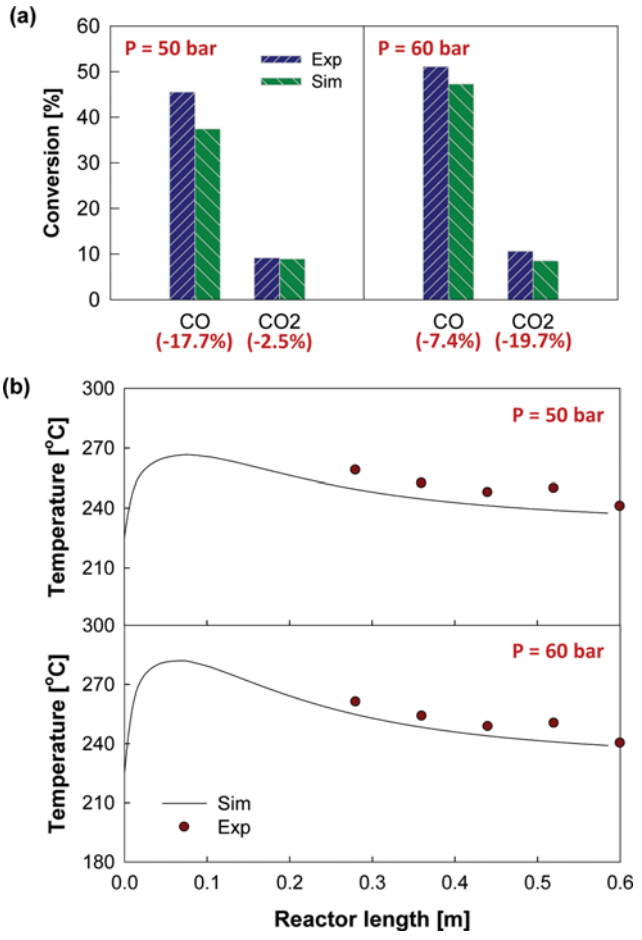

Fig. 4. Comparisons of (a) conversions and (b) temperature profiles between experimental data and simulation results in a bench-scale reactor. Values with parentheses in diagram (a) represent relative errors, and means of absolute relative residuals of temperatures in diagram (b) are 3% and 2.2% for 50 and 60 bar, respectively.

3. Pilot-scale Reactor Modeling

Since the same catalyst pellets were used in both the bench- and the pilot-scale reactors, the value of the effectiveness factor was

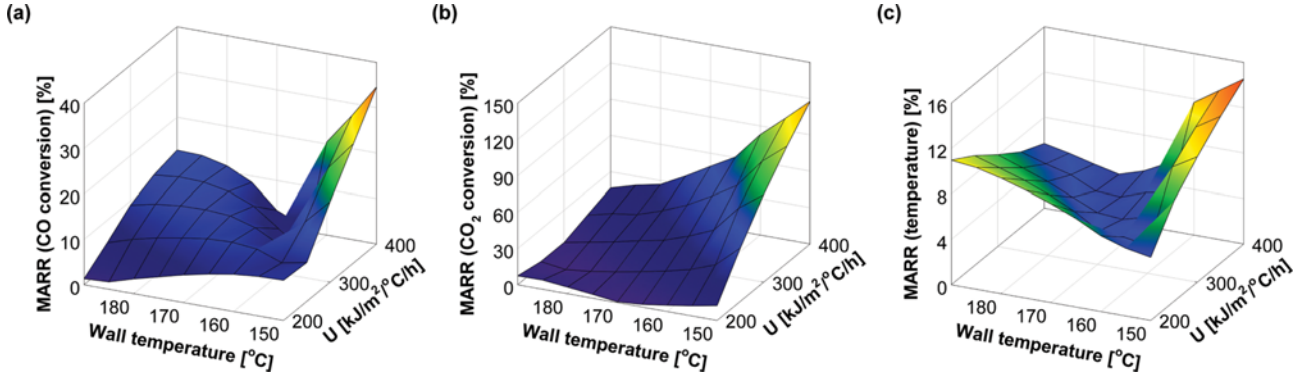

Fig. 5. Effects of wall temperature and overall heat transfer coefficient (U) on the mean of absolute relative residuals (MARR) of (a) CO conversion, (b) CO_2 conversion, and (c) temperature profiles (averaged value of five measurement points) in a pilot-scale reactor.

maintained as 0.5, while the different linear velocity in the pilot-scale reactor required re-estimation of the overall heat transfer coefficient. The effectiveness factor is influenced by operating conditions because different stream velocity affects the thickness of mass transfer boundary layer. However, as discussed in the previous section, the mass transfer was negligible in the present study, while internal diffusion limitation mostly affects the effectiveness factor. In addition, operating temperatures were maintained within limited range. Therefore, constant effectiveness factor was assumed in the pilot-scale reactor.

Because there was no temperature detection in the shell side of the reactor, the wall temperature had to be estimated by fitting the temperature data in the tube side. The latent heat of cooling media was used in the shell side and that the wall temperature was assumed to be constant along the reactor axis. Additionally, the inlet temperature was assumed to be 180 °C, because of the small amount of heat loss in the feeding tube due to incomplete insulation (*cf.* temperature in the feeding tube was measured as 184 °C). Fig. 5 shows the effects of wall temperature and overall heat transfer coefficient (U) on the MARR of conversions and temperature profiles in the pilot-scale reactor. Because the values for minimum MARR for each element were slightly different, as shown in Fig. 5, the optimal value was chosen for balance estimation. The resulting values were 160 °C and 250 kJ/(m^2·°C·h) for wall temperature and overall heat transfer coefficient, respectively, and the corresponding values of MARR were 9.6%, 19.0%, and 4.9% for CO conversion, CO_2 conversion, and temperature, respectively. As shown in Fig. 6, the model satisfactorily describes both conversions and temperature profiles.

To explain different values of overall heat transfer coefficient between bench- and pilot-scale reactors, the correlation for the dimensionless Nusselt number was used [22]:

$$Nu=\frac{hD}{k}=1.86\left(\frac{RePr}{L/D}\right)^{1/3}\left(\frac{\mu}{\mu_S}\right)^{0.14} \quad (10)$$

Here, h, L, D, and k represent the local heat transfer coefficient, tube length, tube diameter, and thermal conductivity, and Re and Pr denote the dimensionless Reynolds number and the Prandtl number, respectively. The symbol μ is viscosity, and the subscript s was used for the fluid viscosity at the heat-transfer boundary surface temperature. As the linear velocity of the pilot-scale reactor was approximately six-times higher than that of the bench-scale reactor, the local heat transfer coefficient was expected to increase 1.8-times. The estimated values for the bench- and pilot-scale reactors were 122 and 250 kJ/(m^2·°C·h), resulting in a ratio of approximately 2, which is close to 1.8. This feature can be applied further to the design of a larger-scale (commercial) reactor, in such a way that overall heat transfer might be predicted approximately and the temperature profile in the reactor as well as the methanol productivity can be calculated. If the heat transfer coefficient becomes a function of linear velocity along the reactor axis (the UniSim Design Suite simulator in the present study allowed to specify the coefficient as constant only), the deviations in Fig. 6(b) might have decreased because the simulated temperature in low temperature region might increase due to the decreased heat transfer coefficient and vice versa.

4. Effects of Operating Conditions in the Open-loop Case

Using the developed model, the effects of operating conditions were evaluated on the methanol production, in the open-loop case. Since the pressure in the shell side was fixed, the wall temperature was assumed to be maintained, while inlet temperature was specified as a manipulated variable. Another condition of interest was feed flowrate (or space velocity), because it directly affects the conversion and methanol productivity. As shown in Fig. 7, both inlet temperature and feed flowrate showed positive effects on the peak temperature (maximum temperature along the axis of the catalytic bed). As feed flowrate increases, all the conversions (CO, CO_2 and H_2) decreased due to the reduced residence time (Figs. 7(d)-7(f)), while methanol production rate, which is the product of yield and feed flowrate, increased due to the increase in the feed flowrate. As a result, maximum methanol production rate was achievable at high inlet temperature as well as high feed flowrate. However, the maximum production corresponded to too high peak temperature (more than 260 °C in Fig. 7(a)), which may result in thermal instability of the reaction system. Because the reactor was designed for the production rate of ten tons per day (TPD), the minimum peak temperature along the 10 TPD line (marked by a red-triangle in Fig. 7(a)) was chosen, and then 10 °C was assumed as a margin, indicating that 250 °C was the maximum allowable peak temperature. Shaded area in Fig. 7 represents the region where peak temperature is below 250 °C and methanol production rate is higher than 10 TPD. Within this operating window, maximum methanol

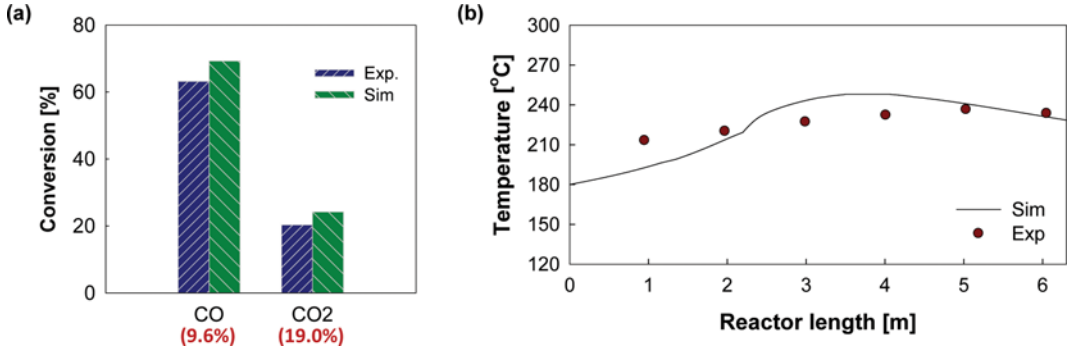

Fig. 6. Comparisons of (a) conversions and (b) temperature profiles between experimental data and simulation results in a pilot-scale reactor. Parentheses in the diagram (a) represent relative errors.

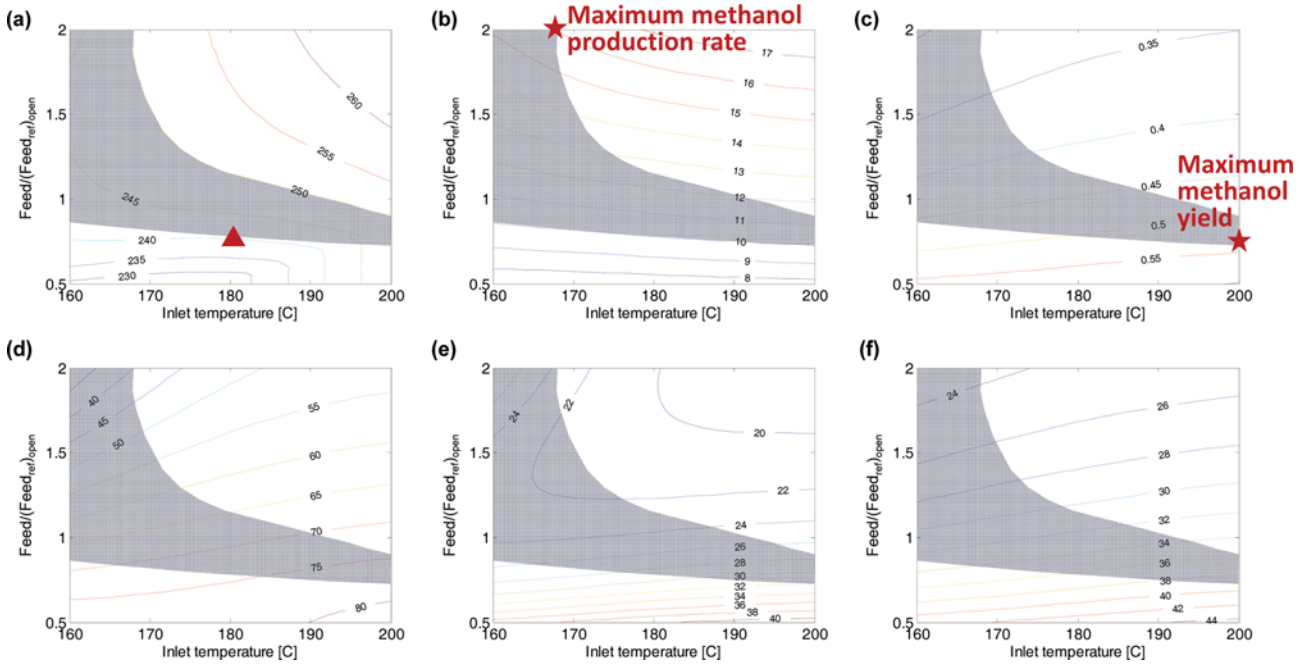

Fig. 7. Contour plots of (a) peak temperature, (b) methanol production rate [ton/day], (c) methanol yield, (d) CO conversion, (e) CO_2 conversion, and (f) H_2 conversion, with respect to inlet temperature and feed flowrate (Feed/(Feed$_{ref}$)$_{open}$) where (Feed$_{ref}$)$_{open}$=178.9 kmol/h, for the open-loop case. Shaded area corresponds to the region where peak temperature is below 250 °C and methanol production rate is higher than 10 tons per day.

production rate of 15.8 TPD was achieved at inlet temperature of 166 °C and feed flowrate of twice of the reference value ((Feed$_{ref}$)$_{open}$= 178.9 kmol/h). Meanwhile, maximum yield required high temperature (200 °C) and low feed flowrate (75% of (Feed$_{ref}$)$_{open}$). Thus, if operation is conducted under the condition for the maximum methanol production rate, the corresponding yield decreases to approximately 0.32, resulting in large amount of unreacted feed gas and probably highly expensive separation cost.

5. Maximum Methanol Production in the Recycled Operation

To prevent the loss of unreacted gases, a recycle stream was introduced in the reactor (Fig. 8), and the simulation was conducted using the same process simulator for reactor modeling (UniSim Design Suite, Honeywell Inc.). The size of the reactor was maintained to be the same in the open-loop case, while additional unit operations were considered in the recycled case: The reactor effluent was cooled to 42 °C by assuming the temperature of cooling water was 32 °C and specifying the minimum approach temperature to be 10 °C (COOLER), and the condensed methanol and water were separated in the SEPARATOR while unreacted gases were recycled to the MIXER. The mixture of feed and recycled gas was heated to the specified value of inlet temperature.

The flowrate for the maximum methanol production in the open-loop was determined to 357.7 kmol/h (=2(Feed$_{ref}$)$_{open}$ in Fig. 7(b)). Meanwhile, since the reactor inlet flowrate in the recycled case was composed of two streams, feed and recycle, therefore, the flowrate of Feed was adjusted so that the reactor inlet (F+R) could be close to 357.7 kmol/h. As a result, the flowrate of feed was determined to be 93.0 kmol/h, which was used as a reference flowrate in the recycled operation (denoted as (Feed$_{ref}$)$_{recycle}$ as in Table 3). The corresponding reactor inlet flowrate was 359.3 kmol/h. As shown in Table 3, despite almost the same space velocity, the methanol production of the reference case in the recycled operation

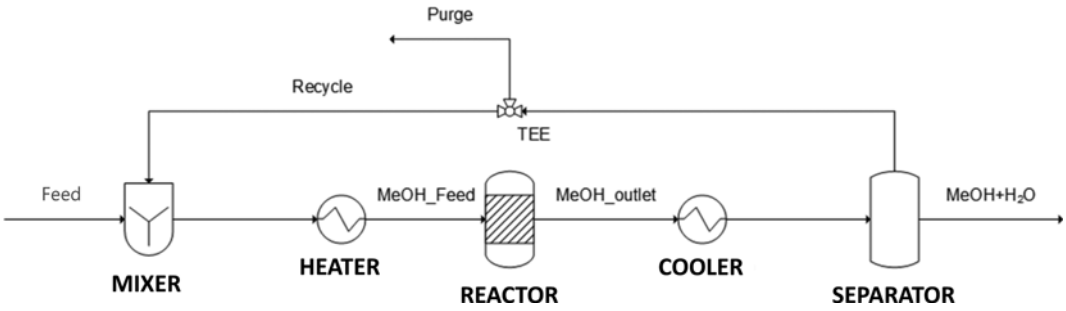

Fig. 8. Scheme of a methanol production with recycled and purge streams.

Table 3. Conditions and results for the open and recycled cases

	Inlet temperature [°C]	Flowrate [kmol/h]			Conversion [%]			Peak temperature [°C]	MeOH production rate [TPD]
		Feed (F)	Recycle (R)	Reactor inlet (F+R)	CO	CO_2	H_2		
Maximum methanol production rate (open-loop)	166	357.7	-	357.7	38.0	24.6	23.5	248.6	15.8
Reference (recycled)	166	93.0 $(Feed_{ref})_{recycle}$	266.3	359.3	20.5	45.5	18.6	209.0	9.6
Maximum methanol production rate (recycled)	200	186.0	554.4	740.4	25.1	32.0	16.9	236.1	18.7

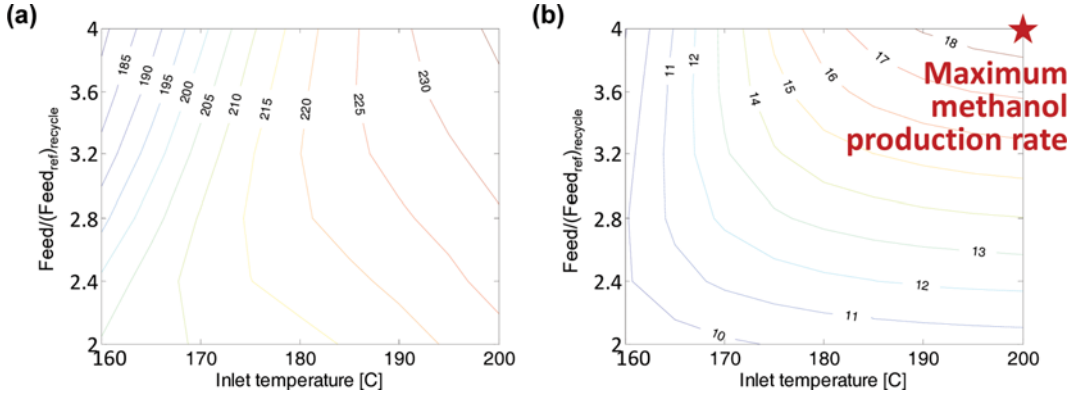

Fig. 9. Contour plots of (a) peak temperature and (b) methanol production rate [ton/day], with respect to inlet temperature and feed flowrate (Feed/$(Feed_{ref})_{recycle}$) where $(Feed_{ref})_{recycle}$=93.0 kmol/h (1,072 kg/h), for the recycled case.

decreased to 9.6. This feature is attributed to the fact that the recycled stream had low CO and CO_2 fraction after separation and included small amount of methanol. Reduced fraction of CO and CO_2 in the reactor inlet led to the decrease in the reaction rate, and the existence of methanol in the inlet increased reverse reaction rate, resulting in the decrease in the net reaction rate. In addition, the reduced reaction rate lowered the peak temperature to 209 °C.

To compensate for the reduced production rate in the reference case of the recycled operation, feed flowrate and inlet temperature were changed. The corresponding peak temperature and methanol production rate are shown by using contour plots in Fig. 9. When the inlet temperature was low (between 160 and 170 °C), the increase of feed flowrate resulted in the decrease of peak temperature, while the production rate increased slightly and then decreased with further increase in the space velocity. Meanwhile, when the inlet temperature was high, the increase of space velocity increased both peak temperature and production rate. As a result, maximum methanol production rate was determined when both inlet temperature and feed flowrate were high. As shown in Table 3, the inlet temperature in the recycled case increased from 166 (open-loop) to 200 °C, and reactor inlet flowrate increased from 357.7 to 740.4 kmol/h. The resulting production rate was 18.7, which was approximately 20% higher value than open-loop case (15.8 TPD). Note that despite exothermic characteristic of the methanol synthesis reaction, the production rate was proportional to inlet temperature, because high space velocity maintained the reaction to be in the kinetic (kinetically controlled) regime, rather than the thermodynamic one.

CONCLUSIONS

A lab-scale-based kinetic model was extended to a pellet-type catalyst for bench- and pilot-scale reactors. The appropriate values of effectiveness factor as well as overall heat transfer coefficient, combined with powder-type catalyst kinetics, clearly described both large-scale reactors. Further analysis showed that the overall heat transfer coefficient, which is one of the important parameters for reactor design, is correlated with linear velocity in the catalytic bed. The developed model could show the operating window for thermally safe and highly productive operation in the open-loop case. In addition, the process with recycled stream to utilize unreacted gas clearly showed that methanol production rate could be further increased with peak temperature maintained below the threshold value. In conclusion, the developed model and parameters can be applied to the design of large-scale reactors and to the determination of the optimal operating conditions in industrial processes.

ACKNOWLEDGEMENTS

This research was supported by the Energy Efficiency & Resources Programs of the KETEP grant funded by the Ministry of Trade, Industry & Energy of the Korean Government (No. 2012T100201578).

REFERENCES

1. G. A. Olah, *Angew. Chem. Int. Ed.*, **44**, 2636 (2005).
2. G. A. Olah and G. K. S. Prakash, US Patent (US7608743 B2) (2009).
3. B. Denise, R. P. A. Sneeden and C. Hamon, *J. Mol. Catal.*, **17**, 359 (1982).
4. P. Mizsey, E. Newson, T. B. Truong and P. Hottinger, *Appl. Catal. A: Gen.*, **213**, 233 (2001).
5. M. Sedighi, M. Ghasemi and A. Jahangiri, *Korean J. Chem. Eng.*, **34**, 997 (2017).
6. H. W. Lim, M. J. Park, S. H. Kang, H. J. Chae, J. W. Bae and K. W. Jun, *Ind. Eng. Chem. Res.*, **48**, 10448 (2009).
7. J. Toyir, P. R. r. de la Piscina, J. L. G. Fierro and N. s. Homs, *Appl. Catal. B: Environ.*, **29**, 207 (2001).
8. J. Wu, S. Luo, J. Toyir, M. Saito, M. Takeuchi and T. Watanabe, *Catal. Today*, **45**, 215 (1998).
9. K. Klier, *Adv. Catal.*, **31**, 243 (1982).
10. G. Natta, in *Catalysis*, P. H. Emmett Eds., Reinhold, New York (1955).
11. M. Takagawa and M. Ohsugi, *J. Catal.*, **107**, 161 (1987).
12. M. Peter, M. B. Fichtl, H. Ruland, S. Kaluza, M. Muhler and O. Hinrichsen, *Chem. Eng. J.*, **203**, 480 (2012).
13. N. Park, M. J. Park, Y. J. Lee, K. S. Ha and K. W. Jun, *Fuel Process. Technol.*, **125**, 139 (2014).
14. D. Kopač, M. Huš, M. Ogrizek and B. Likozar, *J. Phys. Chem. C*, **121**, 17941 (2017).
15. I. Løvik, M. Hillestad and T. Hertzberg, *Comput. Chem. Eng.*, **22**, S707 (1998).
16. H. Kordabadi and A. Jahanmiri, *Chem. Eng. J.*, **108**, 249 (2005).
17. H. Kordabadi and A. Jahanmiri, *Chem. Eng. Process.*, **46**, 1299 (2007).
18. H. W. Lim, H. J. Jun, M. J. Park, H. S. Kim, J. W. Bae, K. S. Ha, H. J. Chae and K. W. Jun, *Korean J. Chem. Eng.*, **27**, 1760 (2010).
19. C. Zhang, K.-W. Jun, R. Gao, G. Kwak and H.-G. Park, *Fuel*, **190**, 303 (2017).
20. J. M. Smith, H. C. Van Ness and M. M. Abbott, *Introduction to Chemical Engineering Thermodynamics*, 7th Ed. McGraw-Hill, New York (2005).
21. H. S. Fogler, *Elements of Chemical Reaction Engineering*, Prentice-Hall, New Jersey (1999).
22. E. N. Sieder and G. E. Tate, *Ind. Eng. Chem.*, **28**, 1429 (1936).
23. G. H. Graaf, P. J. J. M. Sijtsema, E. J. Stamhuis and G. E. H. Joosten, *Chem. Eng. Sci.*, **41**, 2883 (1986).
24. K. L. Ng, D. Chadwick and B. A. Toseland, *Chem. Eng. Sci.*, **54**, 3587 (1999).